



## Research article

# Biosynthesis and characterizations of silver nanoparticles by using green banana peel extract: Evaluation of their antibacterial and electrical performances

Md Ohiduzzaman <sup>a,b,\*</sup>, M.N.I. Khan <sup>c</sup>, K.A. Khan <sup>a,d</sup>, Bithi Paul <sup>e,\*\*</sup><sup>a</sup> Department of Physics, Jagannath University, Dhaka, 1100, Bangladesh<sup>b</sup> Department of Physics, Jashore University of Science and Technology, Jashore, 7408, Bangladesh<sup>c</sup> Materials Science Division, Atomic Energy Centre, Dhaka, Bangladesh<sup>d</sup> Bangamata Sheikh Fojilatunnesa Mujib Science & Technology University, Jamalpur, Bangladesh<sup>e</sup> Department of Physics, American International University-Bangladesh, Dhaka, Bangladesh

## ARTICLE INFO

## Keywords:

Biosynthesis

Ag NPs

Reducing agent

Antibacterial activities

Electricity

## ABSTRACT

Biosynthesized silver nanoparticles (Ag NPs) hold tremendous promise in nano-bioscience, with applications spanning engineering, science, and industry. This study delves into their fabrication process, crystallographic characteristics, and nanostructures. Employing green banana peel extract (GBPE), Ag NPs were synthesized. Various analytical techniques, such as UV-Vis absorption spectrophotometry (UV), X-ray diffraction (XRD), Gas chromatography-mass spectrometry (GC-MS), Field emission scanning electron microscopy (FESEM), Fourier-transform infrared spectroscopy (FTIR), and Transmission electron microscopy (TEM) elucidate their attributes. UV-visible analysis reveals a 413 nm absorption band due to surface plasmon resonance. The Ag NPs exhibit a face-centered cubic structure with an average crystallite size of 45.87 nm. Lattice parameters and dislocation density are also determined. When tested against harmful bacteria, such as *E. coli* and *S. epidermidis*, advanced microscopy reveals a median size of particles of 55.12 nm and demonstrates their antibacterial characteristics. These environmentally benign Ag NPs also improve the efficiency of bio-electrochemical cells (BECs), opening the door to large-scale manufacturing at a reasonable cost and broadening the range of possible uses.

## 1. Introduction

The field of nanotechnology has witnessed significant and potent growth due to its extensive range of applications. Nanomaterials encompass particles with sizes below 100 nm and can be synthesized using straightforward and efficient methods, resulting in a wide array of properties exhibited by various products. The influence of factors such as size, shape, composition, crystallinity, and structure on the properties of metal nanoparticles is widely acknowledged [1–4]. Owing to their exceptional qualities in optical, photocatalytic, electrical, magnetic, and medicinal activities, nanoparticles are becoming more significant in the advancement of nanotechnology throughout several different fields of study [5–7]. The area of nanobiotechnology combines nanotechnology with biological sciences. It offers a framework for the creation of environmentally friendly and green nanoparticle synthesis using biological sources like plants

\* Corresponding author. Department of Physics, Jagannath University, Dhaka, 1100, Bangladesh.

\*\* Corresponding author.

E-mail addresses: [ohid@just.edu.bd](mailto:ohid@just.edu.bd) (M. Ohiduzzaman), [chyabithi@gmail.com](mailto:chyabithi@gmail.com) (B. Paul).<https://doi.org/10.1016/j.heliyon.2024.e31140>

Received 21 February 2024; Received in revised form 9 May 2024; Accepted 10 May 2024

Available online 11 May 2024

2405-8440/© 2024 The Authors. Published by Elsevier Ltd. This is an open access article under the CC BY-NC-ND license (<http://creativecommons.org/licenses/by-nc-nd/4.0/>).

and microbes [8]. In recent years, nanoparticles have become an integral part of our daily lives, finding applications in numerous areas, including transportation, communication, energy storage, sensing, electronics, food production, packaging, medicine, and cosmetics [9,10]. Ag nanoparticles are one of the most viable options among the noble nanomaterials (such as Au, Ag, Pd, and Pt) because of their special functions in electronics, catalysis, materials science, energy, and medicinal applications [11–13].

Bananas, among the most often consumed fruits, are high in nutrients [14]. An estimated 36 million tons of banana peel are generated annually, and because the peel comprises around 35 % of the fruit's weight, it has possible uses [14]. Traditional medicine has employed the peel to cure a variety of conditions, including diarrhea, burns, inflammation, anemia, ulcers, snakebite, diabetes, cough, and excessive menstruation [14–16]. Additionally, the abundance of polymers such as lignin, cellulose, hemicellulose, and pectin present in banana peels can be utilized in the synthesis of Ag NPs [17].

The goal of the current work is to create Ag NPs by a green biological method, especially by using an extract made from leftover banana peels. Additionally, the study focuses on using several analytical methods, such as UV, XRD, FT-IR, TEM, and FESEM analysis, to characterize the produced nanoparticles. The antibacterial effectiveness and electrical activities of Ag NPs are also investigated in the study.

This study suggests that GBPE might be used to manufacture inexpensive, sustainable electrical devices and a bio-reducing agent. The study utilizes GBPE to synthesize Ag NPs and develop BECs for power generation. The BECs utilize a Zn/Cu electrode and peel extract as the electrolyte instead of a chemical electrolyte. The solution containing electrolytes functions better with the addition of GBPE-mediated Ag NPs. Ag NPs catalyze electron flow, boosting energy generation from inorganic and organic molecules to the electrode [18,19,20]. Results showed that the BEC with peel extract electrolyte can generate electricity, and the incorporation of GBPE-mediated Ag NPs decreased the cell's voltage regulation. The internal resistance of the cell reduces, and its open circuit voltage (Voc) and short circuit current (Isc) increase upon the addition of Ag NPs [20–22]. To date, many plant extracts have been utilized as bio electrolyte solution and MnO<sub>2</sub>, Ag NPs have been used as catalysts to improve the performances of cell [13,20,23]. In this report, banana peel extract bio electrolyte solution has been first time investigated in electrochemical cells and the electrical parameters have been examined. Ag NPs from peel extract were tested at different concentrations against *E. coli* and *S. epidermidis*, evaluating their antibacterial properties. The biosynthesized Ag NPs reveal excellent antibacterial properties against both *E. coli* and *S. epidermidis*.

This study innovatively employs banana peel extract and silver nanoparticles in BECs, offering a cost-effective, sustainable approach for renewable energy device development and diverse biological applications.

## 2. Material & methods

### 2.1. GBPE preparation

A recently obtained banana from a local market in Bangladesh was utilized. To generate GBPE, 20 g of the peel underwent boiling in 100 mL of deionized water. Stirring with a magnetic stirrer occurred at 60 °C for 1 h. After cooling, double filtration with Whatman filter papers 41 and 42 removed solid particles. The resulting GBPE was then refrigerated at 4 °C for preservation.

### 2.2. Ag NPs are biosynthesized via the GBPE

Silver ions were reduced by mixing 5 mL of aqueous GBPE with a 0.005 M AgNO<sub>3</sub> solution from Sigma-Aldrich. When kept in the dark, the combination solution changed color over 3.0 h, from colorless to dark brownish. The observed hue change implies that Ag NP was bio-reduced to silver ions. Fig. 1 depicts the Ag NPs synthesis schematic and color changes.

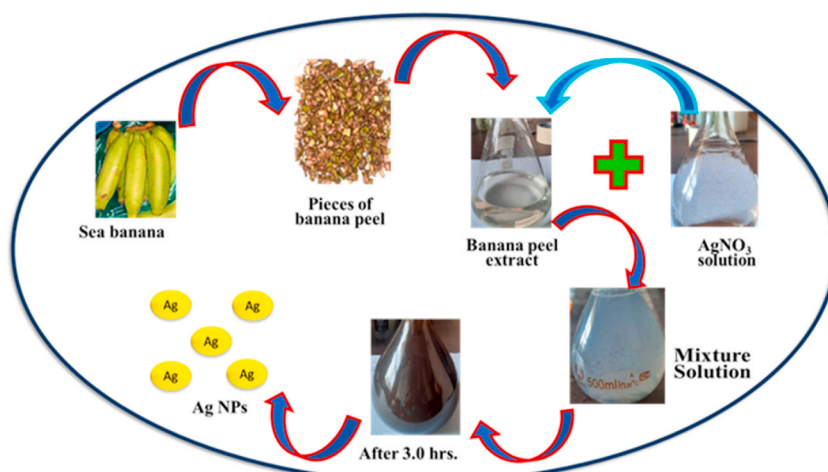


Fig. 1. Biosynthesis of Ag NPs using peel extract as reducing agent.

### 2.3. Characterizations

In Japan, a Rigaku Smart Lab X-ray diffraction device analyzed Ag NPs crystalline structure at  $10^\circ \text{ min}^{-1}$ . The biogenic Ag NPs diffraction pattern was recorded using  $\text{CuK}\alpha$  radiation ( $\lambda = 1.54056 \text{ \AA}$ ). UV-vis analysis (220–1000 nm) employed a U-2900 spectrophotometer, and FTIR identified functional groups. FESEM with a JSM-7610F apparatus revealed the morphology of nanoparticles. Auto-fine platinum coating preceded imaging with a JEC-3000FC coater. The thermo scientific Talos TEM explored the nanostructure of Ag NPs. A PerkinElmer FT-IR spectrophotometer (model L1600300 Spectrum TWO LITA) assessed functional groups in GBPE and Ag NPs from the UK. The Clarus®690 gas chromatograph and Clarus® SQ 8C mass spectrophotometer (PerkinElmer, CA, USA) were employed for GC-MS analysis. Using a  $1 \mu\text{L}$  sample, a split less mode, and pure Helium as the carrier gas, the system operated with specific temperature parameters and a 40-min runtime. Compound identification utilizes the NIST database.

### 2.4. Antibacterial assay

Disc diffusion experiments on Mueller-Hinton agar were used to assess the antibacterial effectiveness of Ag NPs. At a concentration of  $1 \times 10^8 \text{ CFU/mL}$ , bacterial strains from the Microbiology Department of Jashore University of Science and Technology were used. Following a 24-h incubation period at  $37^\circ \text{C}$ , discs containing  $10 \mu\text{l}$  of extract solution containing two doses of Ag NPs were loaded. To evaluate the antibacterial activity, the widths of the inhibition zones were evaluated.

### 2.5. Designing GBPE-electrochemical cell structures

The experiment utilized four BECs to study the effect of Ag NPs on electricity generation. Fig. 2 illustrates cell design, and Table 1 details the electrolyte mixtures. Plates of zinc and copper with similar surface areas were selected.

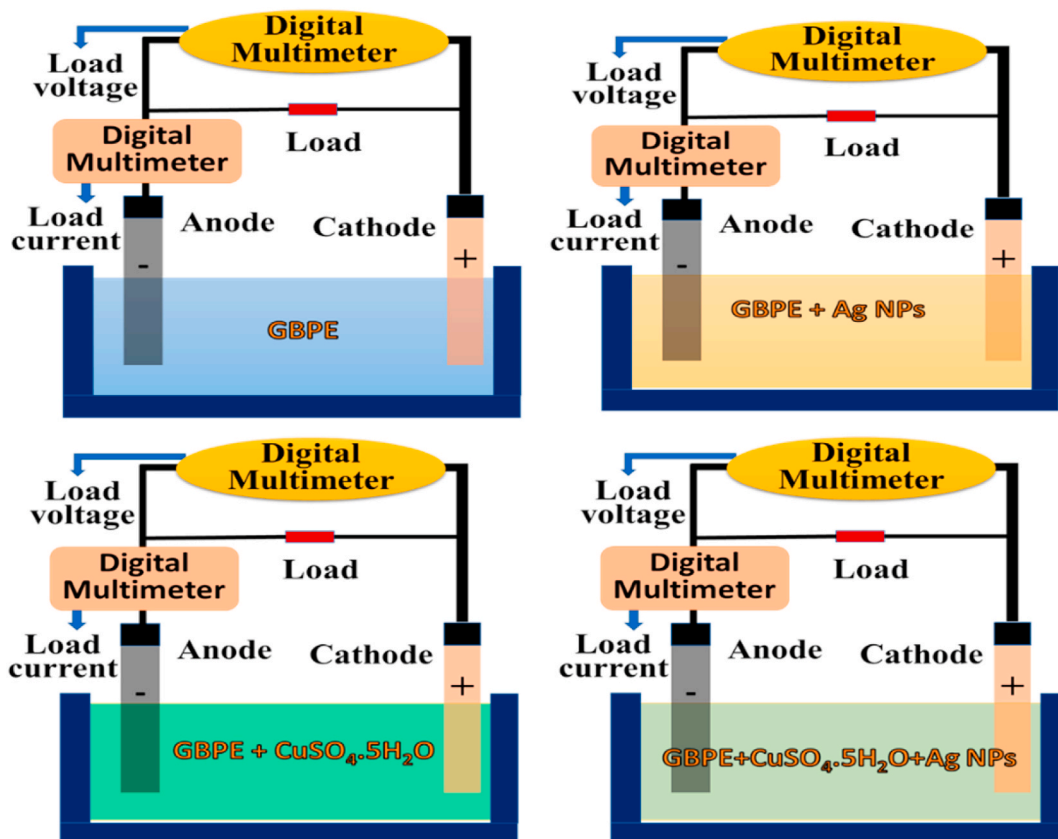


Fig. 2. Configuration of the basic Zn/Cu BECs for experimentation.

**Table 1**  
Diverse electrolyte mixtures.

Title of the Cell	Electrodes	Solution of electrolytes for BECs
Cell- A	Zn and Cu plates	100 mL (GBPE) + 1.2 M CuSO <sub>4</sub> ·5H <sub>2</sub> O in 100 mL + 20 mL (2 mg Ag NPs)
Cell- B	Zn and Cu plates	100 mL (GBPE) + 1.2 M CuSO <sub>4</sub> ·5H <sub>2</sub> O in 100 mL
Cell- C	Zn and Cu plates	100 mL (GBPE) + 20 mL (2 mg Ag NPs)
Cell- D	Zn and Cu plates	100 mL (GBPE)

### 3. Result and discussions

#### 3.1. Diffraction of X-rays

In Fig. 3, four distinct diffraction peaks were observed in the XRD analysis at angles of 38.21°, 44.38°, 64.53°, and 77.48°. Peaks matched crystallographic planes (111), (200), (220), and (311) in face-centered cubic silver [6,11,13,24]. The results aligned well with JCPDS database file No. 65–2871 [11,25].

Using Scherr's formula in Eq. (i), the average crystal size of the Ag NPs produced by the bio-reduction process was ascertained,

$$D = \frac{K\lambda}{\beta \cos \theta} \quad (\text{i})$$

$\lambda$  is X-ray wavelength,  $\theta$  is Bragg's angle,  $K$  is the Scherrer constant (0.9–1), and  $\beta$  is FWHM [26–28]. This formula yielded an estimated average crystal size of 45.87 nm.

Bragg's law, expressed as Eq. (ii),

$$2d \sin \theta = n\lambda \text{ Or, } d = \frac{\lambda}{2 \sin \theta} \text{ (for } n = 1) \quad (\text{ii})$$

Eq.(ii) is utilized to determine the distance between neighboring planes in nanostructure of diffraction peaks.

Additionally, Eq. (iii),

$$\frac{1}{d^2} = \frac{h^2 + k^2 + l^2}{a^2} \text{ Or, } a = d \left( \sqrt{h^2 + k^2 + l^2} \right) \quad (\text{iii})$$

facilitates the calculation of the lattice constant by relating it to the Miller indices (hkl) and the interplanar spacing (d) as shown in Table 2 [29]. The average lattice parameter is calculated at 0.4079 nm.

To quantify the dislocations of the crystal structure, the Williamson-Smallman equation provides a convenient way to estimate the dislocation density ( $\delta$ ) in Eq. (iv) [29,30].

$$\delta = \frac{1}{D^2} \quad (\text{iv})$$

Where, average crystal size,  $D = 45.87$  nm. Dislocations significantly influence material properties, distorting the regular atomic arrangement. 0.000476 lines per nm<sup>2</sup>, an extremely low number, was discovered, highlighting the remarkable crystallinity of the artificially created Ag NPs [31].

#### 3.2. UV–vis absorption spectrophotometry

Fig. 4(a and b) displays UV–visible spectra of Ag NPs, AgNO<sub>3</sub>, and DI water, and GBPE. The highest absorbance for Ag NPs occurs at

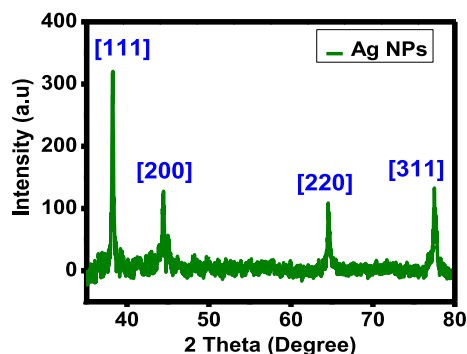
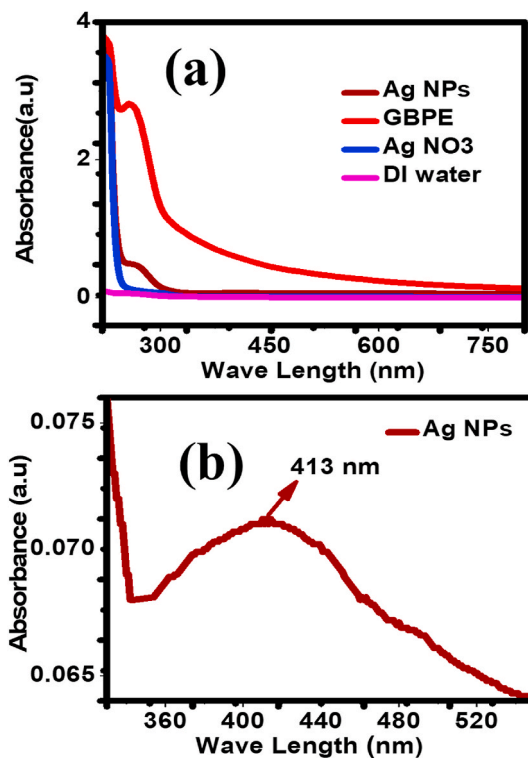


Fig. 3. Pattern of biosynthesized Ag NPs as shown by XRD.

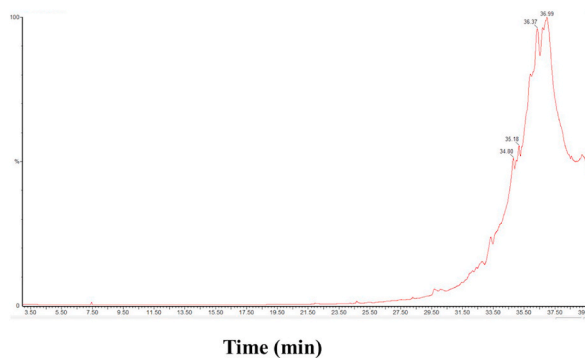
**Table 2**

Presents the measurements of various parameters for the synthesized Ag NPs.

$2\theta$ (°)	FWHM $\beta$ (°)	Miller indices ( <i>hkl</i> )	Crystallite size, D (nm)	Interplanar spacing, d (nm)	Lattice parameter, a (nm)
38.219	0.174	111	48.402	0.235	0.4075
44.390	0.186	200	46.054	0.204	0.4078
64.533	0.206	220	45.540	0.144	0.4081
77.483	0.234	311	43.507	0.123	0.4082

**Fig. 4.** UV-Vis spectra of (a) Ag NPs, banana peel extract, AgNO<sub>3</sub>, DI water; (b) Ag NPs.

413 nm (shown in Fig. 4(a)), indicating surface plasmon resonance (SPR) related to electron oscillation in the conduction band. The addition of AgNO<sub>3</sub> to the peel extract causes a color change from colorless to dark brownish, signifying the conversion of Ag<sup>+</sup> ions to Ag<sup>0</sup> nanoparticles. This conversion relies on reducing agents present in the peel extract, emphasizing their crucial role in Ag NPs formation [26,32].

**Fig. 5.** GBPE ethanol chromatogram by GCMS analysis.

### 3.3. GC-MS analysis

The green banana peel extract underwent GC-MS analysis, revealing 17 identified compounds. The chromatogram in Fig. 5 illustrates this, while Table 3 provides a breakdown of bioactive components with details such as retention times, peak areas, and molecular weights. The primary constituents, notably *trans*-4-*tert*-butylcycloheptanol (39.24%), adipic acid, *cis*-non-3-enyl hexyl ester (0.96%), and 3, 4-altrosan (0.28%), were determined based on their relative abundance in the extract.

### 3.4. FTIR analysis

Ag NPs were investigated in the 400–4000  $\text{cm}^{-1}$  wavenumber range by the FTIR study shown in Fig. 6. The graph revealed strong peaks at approximately 1616  $\text{cm}^{-1}$  for banana peel powder (BPP) and 1628  $\text{cm}^{-1}$  for Ag NPs. These peaks can be linked to the OH bending brought on by bound water as well as the stretching vibration of C=O and C=C bonds [9,33,34]. The stretching vibration of the C–O–H and –CO bonds, as well as the aromatic C–H stretching vibration, are responsible for another band that was seen at about 1014  $\text{cm}^{-1}$  for BPP and 1034  $\text{cm}^{-1}$  for Ag NPs [35–37]. The hydroxyl group (–OH) stretching vibration may be the reason for the peaks seen at 3284  $\text{cm}^{-1}$  for BPP and 3348  $\text{cm}^{-1}$  for Ag NPs [32,38]. The shorter vibration of the HC groups and the stretching bands of the C–H bonds are responsible for the peaks observed at 2970  $\text{cm}^{-1}$  in Ag NPs and 2922  $\text{cm}^{-1}$  in BPP [33,34,36]. The stretching vibrations of C–O bonds are responsible for the band at 1240  $\text{cm}^{-1}$  for BPP and 1290  $\text{cm}^{-1}$  for Ag NPs [39]. Peaks around 808  $\text{cm}^{-1}$  relate to cellulose C–H vibrations, and the 542  $\text{cm}^{-1}$  band is associated with C=H bending and Ag–O bonds [32,40].

### 3.5. Morphological analysis

Plant extracts offer a means to control the levels of agents involved in capping, reducing, and stabilizing, thus influencing the size and shape of metallic NPs [41–43]. Interestingly, during the synthesis process, the extract played a dual role by functioning both as a capping agent and a reducing agent. This dual functionality played a crucial role in preventing excessive aggregation of nanoparticles, and ensuring their long-term stability. Fig. 7(a–d) represents the high-resolution FESEM, TEM images, and particle size distribution. The image indicates that the Ag NPs have a spherical shape, although some also exhibit irregular forms. To assess the size distribution of the Ag NPs generated, an analysis was carried out using ImageJ software. The results indicate that the average particle size is approximately 55.12 nm from FESEM images and around 56.12 nm from TEM images.

## 4. Antibacterial activity of biosynthesized Ag NPs

GBPE mediated Ag NPs exhibited notable antimicrobial activity against *E. coli* and *S. epidermidis* at 200 and 400  $\mu\text{g}/\text{disk}$  concentrations, compared to the ethanol control [23,44,45]. Fig. 8(a–c) depicts Ag NPs strong antibacterial impact, inhibition zones grow with higher concentrations post-24-h incubation at 37 °C. Interestingly, in line with the NP concentrations, *E. Col* showed a bigger inhibitory zone than *S. epidermidis*. Table 4 displays inhibition zone sizes; statistical analysis was conducted. Ag NPs exhibited dose-dependent efficacy against *E. coli* ( $18.55 \pm 0.49$  mm and  $24.6 \pm 0.28$  mm) compared to standard antibiotics. For *S. epidermidis*, Ag NPs zones were  $15.00 \pm 0.71$  mm and  $19.4 \pm 0.57$  mm, while the standard antibiotic had a  $21.35 \pm 0.49$  mm zone. These findings underscore the unique influence of Ag NPs on bacterial development, highlighting their encouraging antibacterial potential against pathogenic bacteria. Crucially, the research excluded any combination or synergistic effects and concentrated only on the individual

**Table 3**  
Analyzing GBPE components with GC-MS.

Serial No.	Retention time (RT)	Compounds	Molecular weight	Molecular Formula	Peak area (%)
1	7.44	Hentriacontane	436	C <sub>31</sub> H <sub>64</sub>	0.05
2	8.81	12-bromododecanoic acid	278	C <sub>12</sub> H <sub>23</sub> O <sub>2</sub> Br	0.01
3	9.96	7-nonenic acid, methyl ester	170	C <sub>10</sub> H <sub>18</sub> O <sub>2</sub>	0.01
4	11.32	1-propen-3-imine, n-cyclohexyl-, n-oxide	153	C <sub>9</sub> H <sub>15</sub> ON	0.05
5	15.23	3-ethoxy-1,1,1,7,7,7-hexamethyl-3,5,5-tris(trimethylsiloxy) tetrasiloxan	562	C <sub>17</sub> H <sub>50</sub> O <sub>7</sub> Si <sub>7</sub>	0.01
6	17.59	Isovaleric acid, nonyl ester	228	C <sub>14</sub> H <sub>28</sub> O <sub>2</sub>	0.01
7	18.94	N-(trifluoroacetyl)-n, o, o', o'-tetrakis(trimethylsilyl) norepinephrine	553	C <sub>22</sub> H <sub>42</sub> O <sub>4</sub> NF <sub>3</sub> Si <sub>4</sub>	0.02
8	21.97	2,2,4-trimethyl-1,3-pentanediol diisobutyrate	286	C <sub>16</sub> H <sub>30</sub> O <sub>4</sub>	0.05
9	24.24	1,1'-bicyclopentyl	138	C <sub>10</sub> H <sub>18</sub>	0.01
10	24.65	Diethyl phthalate	222	C <sub>12</sub> H <sub>14</sub> O <sub>4</sub>	0.06
11	27.02	(Cyclopropyl)trivinylsilane	150	C <sub>9</sub> H <sub>14</sub> Si	0.01
12	27.53	Hexasiloxane, tetradecamethyl-	458	C <sub>14</sub> HO <sub>5</sub> Si <sub>6</sub>	0.02
13	28.29	Tetradecanoic acid, 10,13-dimethyl-, methyl ester	270	C <sub>17</sub> H <sub>34</sub> O <sub>2</sub>	0.03
14	29.68	3,4-altrosan	162	C <sub>6</sub> H <sub>10</sub> O <sub>5</sub>	0.28
15	33.34	Adipic acid, <i>cis</i> -non-3-enyl hexyl ester	354	C <sub>21</sub> H <sub>38</sub> O <sub>4</sub>	0.96
16	35.18	Isopropyl linoleate	322	C <sub>21</sub> H <sub>38</sub> O <sub>2</sub>	0.02
17	36.37	<i>Trans</i> -4- <i>tert</i> -butylcycloheptanol	170	C <sub>11</sub> H <sub>22</sub> O	39.24

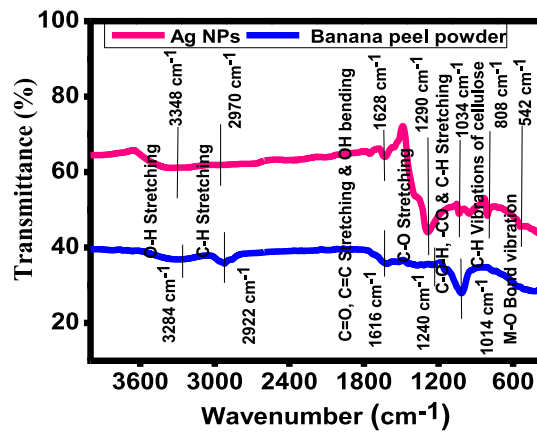


Fig. 6. FT-IR spectrum of Ag NPs and BPP.

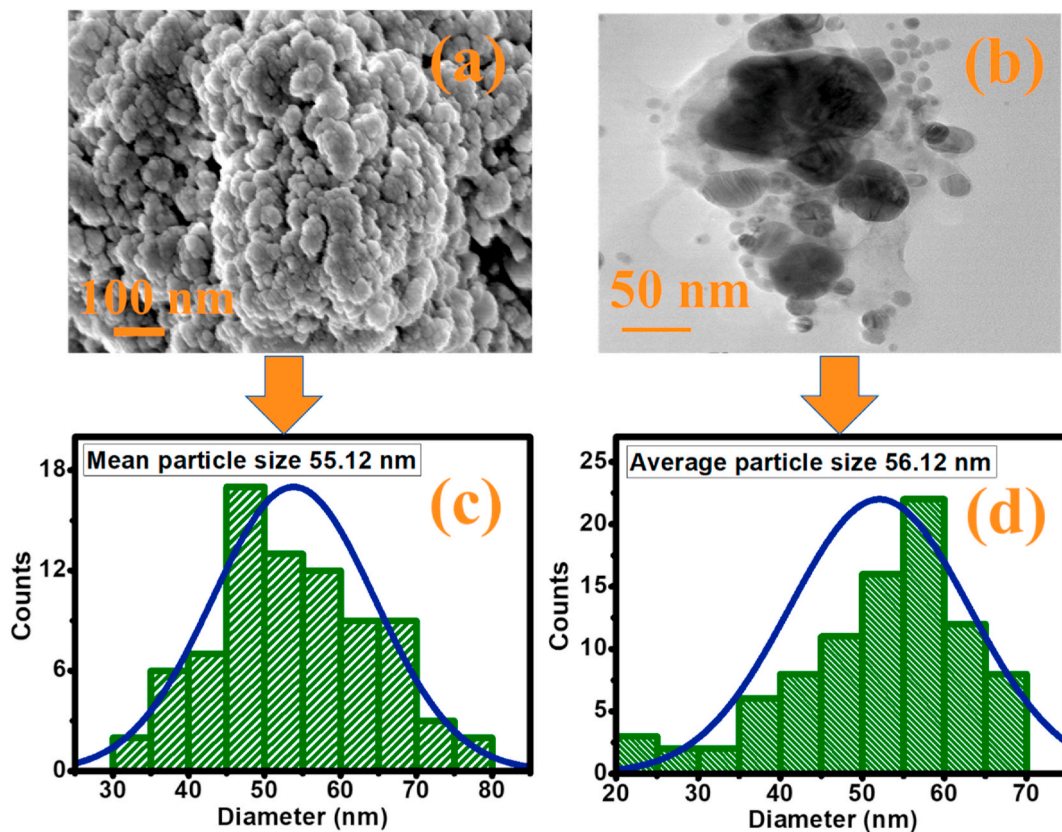


Fig. 7. Morphological images of Ag NPs (a) FESEM image, (b) TEM image, (c) particle size histogram of FESEM image, and (d) particle size histogram of TEM image.

impacts of Ag NPs.

The graph shows the inhibition zones (mm) against bacteria at different doses of the common antibiotic azithromycin (6 mg/mL) and Ag NPs. The impact of Ag NPs at 400 µg/disk (Magenta + Blue) and 200 µg/disk (Orange + Yellow) is represented by error bars (mean ± standard deviation, n = 2), whereas the conventional antibiotic is represented by bars (Green + Olive). The legend highlights specific impacts by making colors more understandable, but the lack of standard errors prevents further in-depth statistical research.

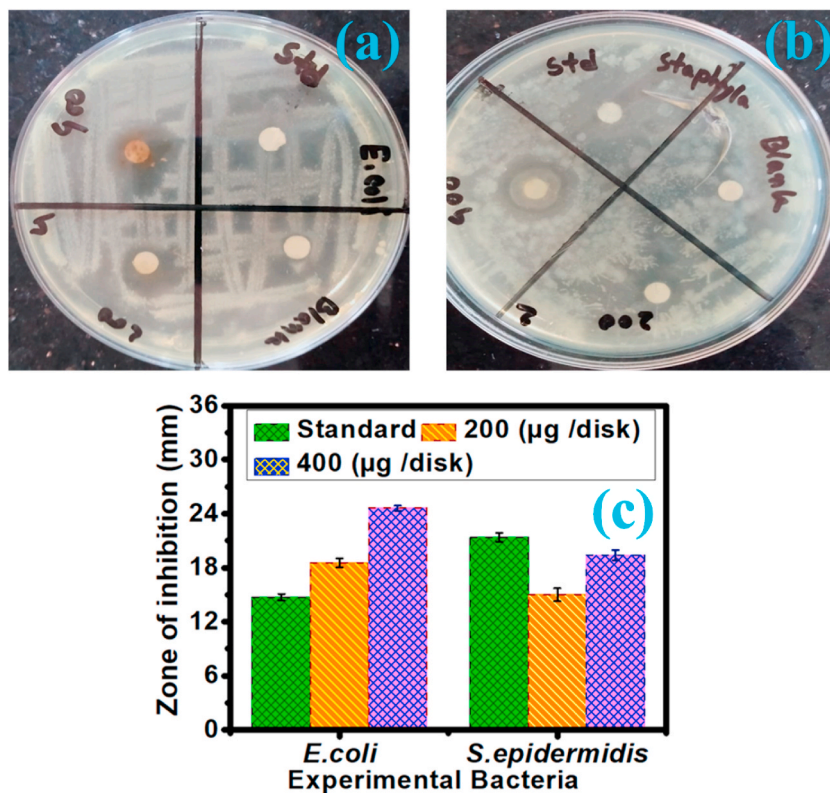


Fig. 8. Displays inhibition zones for Ag NPs, ethanol control, (a) *E. coli*, (b) *S. epidermidis* with images, and (c) bar graphs.

**Table 4**  
Ag NPs antimicrobial properties.

Bacterial variation	Standard antibiotic (Azithromycin) (mm)	The inhibition zone in millimeters	
		Ag NPs (Each concentration has n = 2 replicates)	
		200 µg/disk	400 µg/disk
<i>Escherichia coli</i>	14.75 ± 0.35	18.55 ± 0.49	24.6 ± 0.28
<i>Staphylococcus epidermidis</i>	21.35 ± 0.49	15.00 ± 0.71	19.4 ± 0.57

## 5. Electrical activities of Ag NPs

This study's main goal was to investigate how Ag NPs affect the production of electricity in BECs. Four cells with distinct bio-electrolyte solutions were established and continuously monitored for electrical performance. Fig. 9(a–d) illustrates that all cells, utilizing plant extract electrolytes, generated electricity. Cell-A, with Ag NPs, demonstrated markedly superior open circuit voltage and short circuit current, yielding the highest maximum power output and the lowest internal resistance (0.19 W for Cell-A, 0.02 W for Cell-D). The median electrical performance of Cells A, B, C, and D is summarized in Table 5. In conclusion, the results indicate that Ag NPs can enhance power generation in BECs. Additionally, under a 6 Ω load resistance, Cell-A displayed the lowest voltage regulation value at 0.80, further emphasizing its superior performance.

The rate of electron transportation in such BECs depends on the corrosion rate of Zn plate as well as the  $P^H$  of bio-electrolyte solution [46]. Here, anode Zn releases two electrons to become product ion  $Zn^{2+}$  and these electrons are captured by the reactant ion  $Cu^{2+}$  at the cathode plate. Another reactant ion  $H^+$  is produced from the mild acidic solution of bio-electrolyte. In BECs, as much as reactant ion is produced the cell voltage is increased [20,47,48]. The addition of  $CuSO_4 \cdot 5H_2O$  in the BECs plays an important role in increasing the power production as secondary salt effect [20]. Moreover, the incorporation of Ag NPs in BECs accelerated the flow of electrons during the reaction mechanism as a potential catalyst to increase the electricity generation [13,19,20].

## 6. Conclusions

Unique silver nanoparticles are formed when extract from green banana peels is used because it lowers metal ions. As a reducing

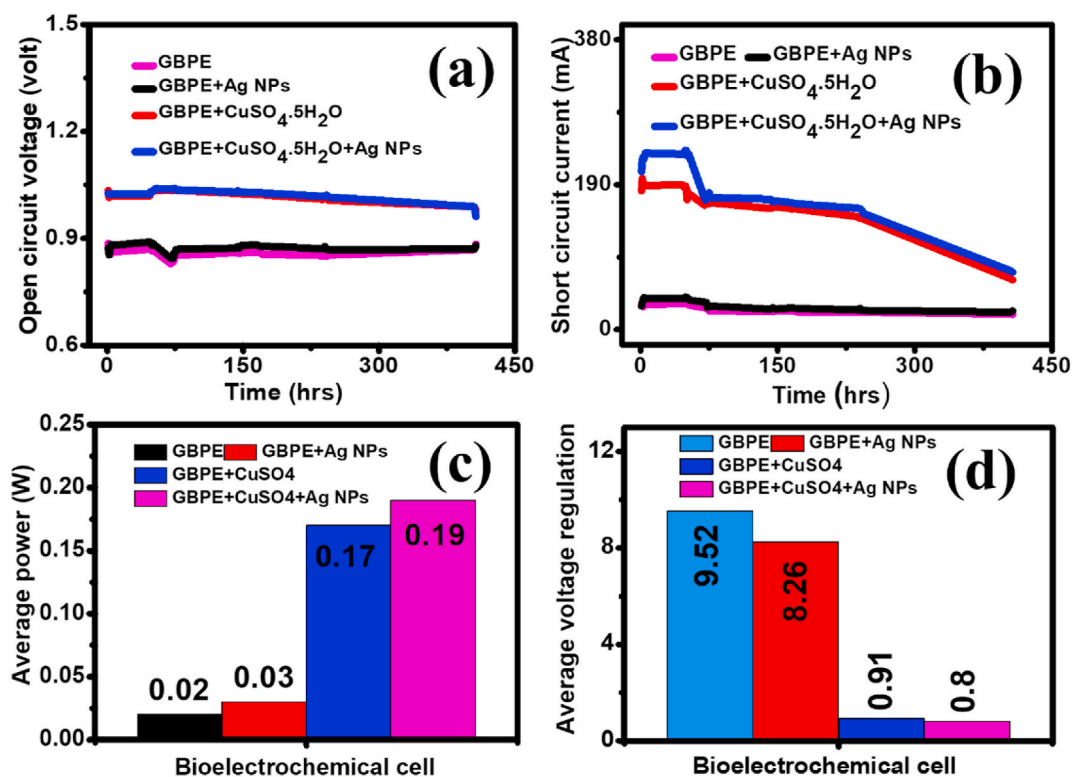


Fig. 9. (a) Voc, (b) Isc, (c) power, and (d) voltage regulation for 6  $\Omega$  load resistance in cell activity.

Table 5

Shows the standard electrical properties of BECs.

Cell's name	Average voltage (volts) of an open circuit	Average short circuit current (A)	Average power (watt)	6 $\Omega$ load resistance mean voltage regulation
Cell- A	1.03	0.18	0.19	0.80
Cell- B	1.02	0.16	0.17	0.91
Cell- C	0.87	0.03	0.03	8.26
Cell- D	0.86	0.02	0.02	9.52

agent, GBPE is essential in converting Ag<sup>+</sup> ions into Ag NPs, as seen by the broad peak for absorption of 413 nm in the UV-visible spectra. XRD analysis was conducted to confirm the synthesized Ag NPs, revealing parameters like lattice parameter, peak indexing, d-spacing, and dislocation density. The resultant average crystalline size was determined to be 45.87 nm, exhibiting an FCC crystalline structure. The participation of certain groups of functions in the reduction process of Ag NPs is further supported by FT-IR spectra. Morphology studies through FE-SEM imagery reveal the spherical shape of Ag NPs, while TEM images validate their synthesis within the 20–70 nm range. Employing the disc diffusion method, the antibacterial efficacy of the synthesized Ag NPs against *E. coli* and *S. epidermidis* was assessed, demonstrating substantial inhibition of both bacterial strains, particularly noticeable against *E. coli*. This suggests the potential of these nanoparticles for medical applications. The investigation of bio-electrolyte cells encompassed four variants, with chemical electrolytes replaced by bio-electrolytes. Remarkably, the integration of Ag NPs into these cells lowered internal resistance, subsequently boosting voltage and current. Cell-A exhibited the least voltage regulation value at 0.80. This study introduces a novel, swift, cost-effective biosynthesis method for Ag NPs, enhancing their applicability in targeted drug delivery, solar cells, water treatment, biosensors, and electronic devices, owing to their small crystal size and catalytic activity.

#### Data availability statement

Data associated with this study have not been deposited into a publicly available repository because all data have been included in this article. The raw data will be made available upon request.

## CRediT authorship contribution statement

**Md Ohiduzzaman:** Writing – original draft, Visualization, Methodology, Investigation, Funding acquisition, Formal analysis, Data curation, Conceptualization. **M.N.I. Khan:** Writing – review & editing, Supervision, Funding acquisition. **K.A. Khan:** Writing – review & editing, Supervision, Funding acquisition, Conceptualization. **Bithi Paul:** Writing – review & editing, Investigation, Formal analysis, Conceptualization.

## Declaration of competing interest

The authors declare the following financial interests/personal relationships which may be considered as potential competing interests Md Ohiduzzaman reports financial support was provided by Government of the People's Republic of Bangladesh Ministry of Science and Technology. If there are other authors, they declare that they have no known competing financial interests or personal relationships that could have appeared to influence the work reported in this paper.

## Acknowledgments

This work is supported by the NST (National Science and Technology) Fellowship, Ministry of Science and Technology, Government of Bangladesh (GoB) (Award Id: 120005100-3821117). The authors would like to acknowledge the Atomic Energy Centre, Dhaka, and Jashore University of Science and Technology, Jashore-7408, Bangladesh to provide the required facilities during this research.

## References

- [1] H. Veisi, S. Azizi, P. Mohammadi, Green synthesis of the silver nanoparticles mediated by *Thymbra spicata* extract and its application as a heterogeneous and recyclable nanocatalyst for catalytic reduction of a variety of dyes in water, *J. Clean. Prod.* 170 (Jan. 2018) 1536–1543, <https://doi.org/10.1016/j.jclepro.2017.09.265>.
- [2] S. Kumar, et al., Plant extract mediated silver nanoparticles and their applications as antimicrobials and in sustainable food packaging: a state-of-the-art review, *Trends Food Sci. Technol.* 112 (Jun. 2021) 651–666, <https://doi.org/10.1016/j.tifs.2021.04.031>.
- [3] X.-F. Zhang, Z.-G. Liu, W. Shen, S. Gurunathan, Silver nanoparticles: synthesis, characterization, properties, applications, and therapeutic approaches, *IJMS* 17 (9) (Sep. 2016) 1534, <https://doi.org/10.3390/ijms17091534>.
- [4] A. Heuer-Jungemann, et al., The role of ligands in the chemical synthesis and applications of inorganic nanoparticles, *Chem. Rev.* 119 (8) (Apr. 2019) 4819–4880, <https://doi.org/10.1021/acs.chemrev.8b00733>.
- [5] M. Darroudi, M. Mansour Bin Ahmad, A.H. Abdullah, N.A. Ibrahim, K. Shameli, Green synthesis and characterization of gelatin-based and sugar-reduced silver nanoparticles, *IJN* (Mar. 2011) 569, <https://doi.org/10.2147/IJN.S16867>.
- [6] M. Shahriary, H. Veisi, M. Hekmati, S. Hemmati, In situ green synthesis of Ag nanoparticles on herbal tea extract (*Stachys lavandulifolia*)-modified magnetic iron oxide nanoparticles as antibacterial agent and their 4-nitrophenol catalytic reduction activity, *Mater. Sci. Eng. C* 90 (Sep. 2018) 57–66, <https://doi.org/10.1016/j.msec.2018.04.044>.
- [7] S.S. Shankar, A. Rai, A. Ahmad, M. Sastry, Rapid synthesis of Au, Ag, and bimetallic Au core–Ag shell nanoparticles using Neem (*Azadirachta indica*) leaf broth, *J. Colloid Interface Sci.* 275 (2) (Jul. 2004) 496–502, <https://doi.org/10.1016/j.jcis.2004.03.003>.
- [8] G. Li, et al., Fungus-mediated green synthesis of silver nanoparticles using *Aspergillus terreus*, *IJMS* 13 (1) (Dec. 2011) 466–476, <https://doi.org/10.3390/ijms13010466>.
- [9] T. Meenatchi, A. Palanimurugan, A. Dhanalakshmi, V. Maheshkumar, B. Natarajan, Green synthesis of *Cynodon Dactylon* capped concentrations on ZnO nanoparticles for antibacterial activity, ROS/ML-DNA treatment and compilation of best controlling microbes by mathematical comparisons, *Chem. Phys. Lett.* 749 (Jun. 2020) 137429, <https://doi.org/10.1016/j.cplett.2020.137429>.
- [10] A.H. Moharram, S.A. Mansour, M.A. Hussein, M. Rashad, Direct precipitation and characterization of ZnO nanoparticles, *J. Nanomater.* 2014 (2014) 1–5, <https://doi.org/10.1155/2014/716210>.
- [11] N. Jayaprakash, et al., Green synthesis of Ag nanoparticles using Tamarind fruit extract for the antibacterial studies, *J. Photochem. Photobiol. B Biol.* 169 (Apr. 2017) 178–185, <https://doi.org/10.1016/j.jphotobiol.2017.03.013>.
- [12] V. Selvaraj, S. Sagadevan, L. Muthukrishnan, Mohd R. Johan, J. Podder, Eco-friendly approach in synthesis of silver nanoparticles and evaluation of optical, surface morphological and antimicrobial properties, *J Nanostruct Chem* 9 (2) (Jun. 2019) 153–162, <https://doi.org/10.1007/s40097-019-0306-9>.
- [13] M.A. Hossain, B. Paul, K.A. Khan, M. Paul, M.A. Mamun, M.E. Quayum, Green synthesis and characterization of silver nanoparticles by using *Bryophyllum pinnatum* and the evaluation of its power generation activities on bio-electrochemical cell, *Mater. Chem. Phys.* 282 (Apr. 2022) 125943, <https://doi.org/10.1016/j.matchemphys.2022.125943>.
- [14] H.T. Vu, C.J. Scarlett, Q.V. Vuong, Optimization of ultrasound-assisted extraction conditions for recovery of phenolic compounds and antioxidant capacity from banana (*Musa cavendish*) peel, *J. Food Process. Preserv.* 41 (5) (Oct. 2017) e13148, <https://doi.org/10.1111/jfpp.13148>.
- [15] H.T. Vu, C.J. Scarlett, Q.V. Vuong, Phenolic compounds within banana peel and their potential uses: a review, *J. Funct. Foods* 40 (Jan. 2018) 238–248, <https://doi.org/10.1016/j.jff.2017.11.006>.
- [16] A. Pereira, M. Maraschin, Banana (*Musa spp*) from peel to pulp: ethnopharmacology, source of bioactive compounds and its relevance for human health, *J. Ethnopharmacol.* 160 (Feb. 2015) 149–163, <https://doi.org/10.1016/j.jep.2014.11.008>.
- [17] Pranalal Rajendra Gunjal, Shital Dnyaneshwar Gaikwad, Green synthesis and characterization of silver nanoparticles using banana peel extract and their biological activity against representative microorganism, *World J. Bio. Pharm. Health Sci.* 13 (1) (Jan. 2023), <https://doi.org/10.30574/wjbps.2023.13.1.0048>, 425–239.
- [18] K.A. Khan, et al., Bioelectrical characterization and production of nanoparticles (NPs) using PKL extract for electricity generation, *Microsyst. Technol.* 28 (3) (Mar. 2022) 823–832, <https://doi.org/10.1007/s00542-020-04774-0>.
- [19] Md Ohiduzzaman, M.N.I. Khan, K.A. Khan, Bithi Paul, Biosynthesis of silver nanoparticles by banana pulp extract: characterizations, antibacterial activity, and bioelectricity generation, *Heliyon* (Feb. 2024) e25520, <https://doi.org/10.1016/j.heliyon.2024.e25520>.
- [20] M. Ohiduzzaman, M.N.I. Khan, K.A. Khan, B. Paul, Green synthesis of silver nanoparticles by using *Allium sativum* extract and evaluation of their electrical activities in bio-electrochemical cell, *Nanotechnology* 35 (9) (Feb. 2024) 095707, <https://doi.org/10.1088/1361-6528/ad10e4>.
- [21] M.A. Hossain, M. Ohiduzzaman, R. Sultana, R. Khatun, S. Akter, K.A. Khan, M. Hasan, PKL electricity-an observations, in: *Advances in Medical Physics and Healthcare Engineering: Proceedings of AMPHE 2020*, Springer Singapore, 2021, pp. 555–566, [https://doi.org/10.1007/978-981-33-6915-3\\_53](https://doi.org/10.1007/978-981-33-6915-3_53).
- [22] K.A. Khan, F. Islam, M.S. Hossain, S.R. Rasel, M. Ohiduzzaman, Red spinach-A new and innovative power source, in: *Microelectronics, Circuits and Systems: Select Proceedings of Micro2021*, Springer Nature Singapore, Singapore, Jun 2023, pp. 113–124, [https://doi.org/10.1007/978-981-99-0412-9\\_10](https://doi.org/10.1007/978-981-99-0412-9_10).

- [23] R. Parameshwaran, S. Kalaiselvam, R. Jayavel, Green synthesis of silver nanoparticles using *Beta vulgaris*: role of process conditions on size distribution and surface structure, *Mater. Chem. Phys.* 140 (1) (Jun. 2013) 135–147, <https://doi.org/10.1016/j.matchemphys.2013.03.012>.
- [24] Y.-Y. Dong, Y.-H. Zhu, M.-G. Ma, Q. Liu, W.-Q. He, Synthesis and characterization of Ag@AgCl-reinforced cellulose composites with enhanced antibacterial and photocatalytic degradation properties, *Sci. Rep.* 11 (1) (Feb. 2021) 3366, <https://doi.org/10.1038/s41598-021-82447-2>.
- [25] S. Jebriil, R. Khanfir Ben Jenana, C. Dridi, Green synthesis of silver nanoparticles using *Melia azedarach* leaf extract and their antifungal activities: in vitro and in vivo, *Mater. Chem. Phys.* 248 (Jul. 2020) 122898, <https://doi.org/10.1016/j.matchemphys.2020.122898>.
- [26] J.M. Ashraf, M.A. Ansari, H.M. Khan, M.A. Alzohairy, I. Choi, Green synthesis of silver nanoparticles and characterization of their inhibitory effects on AGEs formation using biophysical techniques, *Sci. Rep.* 6 (1) (Feb. 2016) 20414, <https://doi.org/10.1038/srep20414>.
- [27] A.A. Kulkarni, B.M. Bhanage, Ag@AgCl nanomaterial synthesis using sugar cane juice and its application in degradation of azo dyes, *ACS Sustainable Chem. Eng.* 2 (4) (Apr. 2014) 1007–1013, <https://doi.org/10.1021/sc4005668>.
- [28] S. Sagadevan, et al., Photocatalytic activity and antibacterial efficacy of titanium dioxide nanoparticles mediated by *Myristica fragrans* seed extract, *Chem. Phys. Lett.* 771 (May 2021) 138527, <https://doi.org/10.1016/j.cplett.2021.138527>.
- [29] R.F.N. Quadrado, G. Gohlke, R.S. Oliboni, A. Smaniotto, A.R. Fajardo, Hybrid hydrogels containing one-step biosynthesized silver nanoparticles: preparation, characterization and catalytic application, *J. Ind. Eng. Chem.* 79 (Nov. 2019) 326–337, <https://doi.org/10.1016/j.jiec.2019.07.008>.
- [30] T. Thiawong, K. Onlaor, B. Tunhoo, A humidity sensor based on silver nanoparticles thin film prepared by electrostatic spray deposition process, *Adv. Mater. Sci. Eng.* 2013 (2013) 1–7, <https://doi.org/10.1155/2013/640428>.
- [31] S.S. Gandhad, et al., Synthesis and characterization of silver nanoparticles using green route, *International Journal of Advanced Science and Engineering* 8 (3) (Feb. 2022) 2252, <https://doi.org/10.29294/IJASE.8.3.2022.2252-2259>.
- [32] S. Pugazhendhi, E. Kirubha, P.K. Palanisamy, R. Gopalakrishnan, Synthesis and characterization of silver nanoparticles from *Alpinia calcarata* by Green approach and its applications in bactericidal and nonlinear optics, *Appl. Surf. Sci.* 357 (Dec. 2015) 1801–1808, <https://doi.org/10.1016/j.apsusc.2015.09.237>.
- [33] J.A. García-Ramón, et al., Morphological, barrier, and mechanical properties of banana starch films reinforced with cellulose nanoparticles from plantain rachis, *Int. J. Biol. Macromol.* 187 (Sep. 2021) 35–42, <https://doi.org/10.1016/j.ijbiomac.2021.07.112>.
- [34] T.Í.S. Oliveira, et al., Bionanocomposite films based on polysaccharides from banana peels, *Int. J. Biol. Macromol.* 101 (Aug. 2017) 1–8, <https://doi.org/10.1016/j.ijbiomac.2017.03.068>.
- [35] X. Li, H. Jiang, Y. Pu, J. Cao, W. Jiang, Inhibitory effect of condensed tannins from banana pulp on cholesterol esterase and mechanisms of interaction, *J. Agric. Food Chem.* 67 (51) (Dec. 2019) 14066–14073, <https://doi.org/10.1021/acs.jafc.9b05212>.
- [36] P.A. Méndez, Á.M. Méndez, L.N. Martínez, B. Vargas, B.L. López, Cassava and banana starch modified with maleic anhydride-poly (ethylene glycol) methyl ether (Ma-mPEG): a comparative study of their physicochemical properties as coatings, *Int. J. Biol. Macromol.* 205 (Apr. 2022) 1–14, <https://doi.org/10.1016/j.ijbiomac.2022.02.053>.
- [37] T.D.M. Florian, et al., Chemical composition analysis and structural features of banana rachis lignin extracted by two organosolv methods, *Ind. Crop. Prod.* 132 (Jun. 2019) 269–274, <https://doi.org/10.1016/j.indcrop.2019.02.022>.
- [38] T.S. Alomar, N. AlMasoud, M.A. Awad, M.F. El-Tohamy, D.A. Soliman, An eco-friendly plant-mediated synthesis of silver nanoparticles: characterization, pharmaceutical and biomedical applications, *Mater. Chem. Phys.* 249 (Jul. 2020) 123007, <https://doi.org/10.1016/j.matchemphys.2020.123007>.
- [39] H. Tamaoki, S. Minato, S. Takei, K. Fujisawa, A clinical method for the determination of serum gamma-glutamyl transpeptidase, *Clin. Chim. Acta* 65 (1) (Nov. 1975) 21–27, [https://doi.org/10.1016/0009-8981\(75\)90330-7](https://doi.org/10.1016/0009-8981(75)90330-7).
- [40] M. Abbasi, F. Saeed, U. Rafique, Preparation of silver nanoparticles from synthetic and natural sources: remediation model for PAHs, *IOP Conf. Ser. Mater. Sci. Eng.* 60 (Jun. 2014) 012061, <https://doi.org/10.1088/1757-899X/60/1/012061>.
- [41] T.A. Salih, K.T. Hassan, S.R. Majeed, I.J. Ibraheem, O.M. Hassan, A.S. Obaid, In vitro scolicidal activity of synthesised silver nanoparticles from aqueous plant extract against *Echinococcus granulosus*, *Biotechnology Reports* 28 (Dec. 2020) e00545, <https://doi.org/10.1016/j.btre.2020.e00545>.
- [42] M.A. Bhutkar, D.S. Randive, G.H. Wadkar, S.Y. Kamble, S. Bhinge, Formulation and evaluation of polyherbal gel containing extracts of *Azadirachta indica*, *Adhatoda vasica*, *Piper betle*, *Ocimum tenuiflorum* and *Pongamia pinnata*, *jrp* 23 (1) (Nov. 2018) 44–54, <https://doi.org/10.12991/jrp.2018.107>.
- [43] S. Ahmed, M. Ahmad, B.L. Swami, S. Ikram, A review on plants extract mediated synthesis of silver nanoparticles for antimicrobial applications: a green expertise, *J. Adv. Res.* 7 (1) (Jan. 2016) 17–28, <https://doi.org/10.1016/j.jare.2015.02.007>.
- [44] I.C. Ehrhart, P.E. Parker, W.J. Weidner, J.M. Dabney, J.B. Scott, F.J. Haddy, Coronary vascular and myocardial responses to carotid body stimulation in the dog, *Am. J. Physiol.* 229 (3) (Sep. 1975) 754–760, <https://doi.org/10.1152/ajplegacy.1975.229.3.754>.
- [45] G.W. Kidder, C.W. Montgomery, Oxygenation of frog gastric mucosa in vitro, *Am. J. Physiol.* 229 (6) (Dec. 1975) 1510–1513, <https://doi.org/10.1152/ajplegacy.1975.229.6.1510>.
- [46] Z. Cai, J. Wang, Y. Sun, Anode corrosion in aqueous Zn metal batteries, *eScience* 3 (1) (Feb. 2023) 100093, <https://doi.org/10.1016/j.esci.2023.100093>.
- [47] M. Paul, K.A. Khan, B. Paul, “Comparative study of electrical performances of bio-electrochemical cell” in *Micro and Nanoelectronics Devices*, in: T.R. Lenka (Ed.), *Circuits and Systems in Lecture Notes in Electrical Engineering*, vol. 904, Springer Nature Singapore, Sep. 2023, pp. 199–208, [https://doi.org/10.1007/978-981-19-2308-1\\_21](https://doi.org/10.1007/978-981-19-2308-1_21).
- [48] Y.Y. Dong, Y.H. Zhu, M.G. Ma, Q. Liu, W.Q. He, Synthesis and characterization of Ag@AgCl-reinforced cellulose composites with enhanced antibacterial and photocatalytic degradation properties, *Sci. Rep.* 11 (1) (Feb. 2021) 3366, <https://doi.org/10.1038/s41598-021-82447-2>.